Tracking of Coastal Swell Fields in SAR Images for Sea Depth Retrieval: Application to ALOS L-Band Data

Valentina Boccia, Alfredo Renga, Antonio Moccia, *Senior Member, IEEE*, and Simona Zoffoli

***Abstract*—Swell propagation in shallow water sets specific relationships between water depth and swell parameters like swell wavelength and period. These relationships allow coastal bathymetry to be retrieved if swell parameters are measured. Synthetic aperture radar (SAR) is able to image swell waves, and spectral analysis of SAR images is a well-known approach for measuring swell parameters. However, owing to nonlinearities in SAR imaging, speckle and noise, spectral analysis can result in significant bathymetric errors. The paper individuates the conditions in which linear imaging is achieved and presents an algorithm able to preserve the accuracy of the calculated bathymetry against image speckle and noise. The proposed approach includes: 1) image resizing and filtering before spectral analysis; 2) limitations to the domain of the spectral analysis; and 3) spatial smoothing of the estimated parameters. The algorithm is tested on L-band ALOS PALSAR data collected over coastal regions in the Gulf of Naples, Italy, showing that swell can be properly tracked from open sea to shoreline. Dense coverage and submetric accuracy is thus achieved.**

***Index Terms*—ALOS PALSAR, bathymetry, dispersion relation, swell waves, synthetic aperture radar (SAR).**

I. Introduction

BATHYMETRY is the measurement of depths and shapes of underwater terrains [1]. Bathymetric data are important for oceanography and oceanic science since underwater mountains, basins, and ridges affect the global flow of sea water that transfers heat, but also nutrients and pollutants, among different earth regions. Concerning coastal areas, the knowledge of water depth is essential to guarantee safe navigation. In addition, structure construction, pipeline and cable routing, and siting of underwater power plant require accurate bathymetric data [2], [3]. Finally, the capability to monitor variations in seabed morphology is a prerequisite for the control of geomorphological risk in coastal areas [4], including forecasting of potential flooding events and warp analysis.

The most assessed and mature technology to perform bathymetric measurements is represented by echo-sounders mounted on dedicated ships [5]–[8]. They carry out hydrographic survey campaigns and cover the area of interest by planned straight transects [9]. In this way, they collect a dense distribution of bathymetric data. Subdecimeter depth and geolocation accuracy can be achieved when the echo-sounder is integrated with inertial sensors and differential GPS [10]–[13]. The main drawback of such hydrographic surveys is that they involve high costs, long acquisition times, and repeated acquisition campaigns if bathymetric changes must be monitored over time [14].

Several remote sensing techniques have been proposed as potential alternatives or in support to conventional techniques. Indeed, satellite remote sensing allows large areas to be quickly covered at relatively low cost. With specific reference to electro-optical sensors, the use of passive [15], [16] or light detection and ranging (LIDAR) [17]–[23] technology was proposed. The results have shown that these techniques achieve good performance over clear and very shallow (up to 20 m) waters only [24].

For deeper waters, synthetic aperture radar (SAR) data represent a promising alternative [25]–[27]. SAR microwave signals are not able to penetrate sea surface. SAR images are generated by signals backscattered from sea surface. Nevertheless, bathymetry can be retrieved from SAR data because, under specific conditions, underwater morphology is able to modify the characteristics of sea surface and therefore to introduce modulations into SAR image intensity. These mechanisms are related to the hydrodynamic characteristics of sea motion and are not affected by the quality of the water. Hence, SAR bathymetry can be used independently from the clearness of the water.

Bathymetric measurements can be generated from SAR data using two families of processing techniques provided that a number of conditions are respected. In detail, SAR bathymetry is based on the exploitation of either sea currents or sea waves. The variation in surface current velocity resulting from local depth changes is used in the first case. Indeed, according to the three-step mechanism introduced in [28], surface current gradients produced by depth variations modify the spectrum of short, wind-generated, surface waves, thus leading to modulations in surface roughness, which result in intensity modulations of radar imagery. Current-based algorithms have been diffusely investigated [25], [27]–[32] and some operational solutions have been proposed [14], [33]–[35]. However, applicability of this approach to close areas, e.g., gulfs or inlets, or relative close seas, e.g., the Mediterranean Sea, is very limited because current velocity is too slow or tends to be irregular both in time and in intensity [14].

Manuscript received October 09, 2014; revised February 20, 2015; accepted March 23, 2015. Date of publication April 20, 2015; date of current version August 11, 2015. The work of V. Boccia was supported by Regione Campania in the framework of the project for Technology Innovation of Transport Systems (INSIST).

V. Boccia, A. Renga, and A. Moccia are with the Department of Industrial Engineering, University of Naples "Federico II", Napoli 80125, Italy (e-mail: alfredo.renga@unina.it).

S. Zoffoli is with Italian Space Agency, Rome 00133, Italy (e-mail: simona.zoffoli@asi.i).

Digital Object Identifier 10.1109/JSTARS.2015.2418273

Bathymetric techniques relying on the investigation of gravity waves, or swell, propagation in coastal areas have been recently proposed [24], [36]–[39]. The approach is suitable for close areas and seas where currents are extremely weak and cannot be used to infer bathymetry [39]. Within past works [26], [39], the authors were involved in the implementation and testing of the bathymetric algorithm discussed in [24] and [37] which is the simplest approach for SAR-based bathymetry by swell analysis. The algorithm is a direct application of the theory of swell propagation assuming that SAR data can be interpreted as a two-dimensional (2-D) picture of sea surface. This algorithm is referred to as theory-driven algorithm in the remainder of the present paper. The application to SAR data showed that unstable and inaccurate depth measurements can result from the theory-driven algorithm [39], [40]. The present paper focuses on understanding the limitations of this algorithm and on integrating it with additional processing steps to achieve more robust, reliable, and accurate bathymetric data retrieval [40], [41].

This paper is organized as follows. Section II describes the effects of seabed morphology on the propagation of swell waves and the basic theory for bathymetric data retrieval from swell parameters. Section III presents the mechanism of SAR imaging of swell waves and the relevant, theory-driven, algorithm for SAR-based bathymetry. Section IV describes the proposed algorithm for reliable tracking of swell waves and bathymetric data retrieval. Finally, Section V presents the experimental results obtained by applying the proposed algorithm to ALOS PALSAR L-band SAR data collected over the Gulf of Naples, Italy.

II. Swell Waves and Bathymetry

The profile of sea surface in stationary conditions can be modeled as a sum of infinite harmonic components, each of them characterized by specific values of parameters such as amplitude, phase, angular frequency and period, and wavenumber and wavelength. Based on wave features and dynamics, and with specific reference to SAR observation of sea, three main kinds of waves can be defined [42], [43], namely capillarity waves, wind sea, and swell waves. Capillarity waves or ripples are wind-generated waves, characterized by very high-frequency and irregular patterns. Wind sea waves are more regular and longer than ripples, but still include wind-generated high-frequency components. Swell waves, on the contrary, generate in a certain region of sea surface as the result of intense and adverse weather conditions. Their propagation is dominated by gravity and is not significantly affected by wind. For this reason, they are able to propagate far from their region of origin and can continue travelling for several days. Swell waves are characterized by long period and long individual crests which tend to be uniform in height, period, and direction of propagation [43]–[45]. Swell waves' characteristics change when they travel from deep to shallow water due to the influence of seabed morphology. Typically, alterations occur starting from intermediate water depth, i.e., when sea water depth is shorter than about half of swell wavelength [37].

Effects of sea bottom morphology on swell waves' characteristics in intermediate water depth can be essentially related to the following two main phenomena [43], [46]: shoaling and refraction.

Shoaling phenomenon occurs when swell waves travel from deep to intermediate water. In such a condition, swell wavelength decreases and swell height increases due to conservation of energy. Concerning refraction, when the crests of swell waves are not aligned with the iso-depth lines of local seabed, magnitude of shoaling phenomenon varies along each crest. Indeed, different portions of the crest travel at different speeds and the parts in shallower water result to be more decelerated than those in deeper water. Hence, the direction of swell propagation changes and the final result is a realignment of swell crests that tend to become parallel to the iso-depth lines of the bottom topography. Refraction and shoaling continue until swell crests are aligned with the iso-depth lines or they break [37], [46].

Investigation of swell shoaling and refraction phenomena in intermediate water can be used to indirectly infer sea water depth and seabed morphology in coastal areas. It is clear that a suitable mathematical model must be introduced. Specifically, swell waves' parameters and sea water depth can be related through the so-called dispersion relation for swell waves [43]–[45]. This relation takes into account the physical processes governing the hydrodynamic phenomenon of modulation of swell waves due to water depth variations. Extensive studies have been performed on this relation and several mathematical expressions have been formulated, each with a different level of detail [3], [44], [47], [48].

The dispersion relation defines the angular frequency of swell waves, i.e., the swell waves' oscillation frequency as evaluated by an observed fixed in the medium, as a function of sea-state parameters. The finite depth linear version of the dispersion relation for swell waves, i.e., the linear dispersion relation, is based on the Airy wave theory [49]. This linear wave theory well represents the mechanism of swell waves propagating on the surface of a homogeneous fluid layer under the assumption of small amplitude waves. A sinusoidal swell wave profile is adopted in this theory without losing generality since more complex swell wave profiles can be obtained from superposition of sinusoidal waves with different values of wavelength. The standard expression of the linear dispersion relation in intermediate water depth relates the swell wave frequency to the swell wavenumber and to the sea water depth h, through the control force of swell waves propagation, i.e., gravity acceleration g. If values of swell wavelength L and swell period T are considered, the following linear dispersion relation depth can be formulated:

$$h = \frac{L}{2\pi}\tanh^{-1}\left(\frac{2\pi L}{T^2 g}\right), \quad \frac{L}{20} < h < \frac{L}{2}. \tag{1}$$

Equation (1) is valid in intermediate water, i.e., when the depth ranges from 1/20 and half the wavelength. According to the linear dispersion relation, when values of swell wavelength and period are known, sea water depth can be estimated.

Similarly, nonlinear dispersion relations have been proposed [4], [44], [45], [47], [48]. However, experimental results have shown that when nonlinear wave theories are adopted, uncertainty in the retrieved sea water depth is larger than the one achieved with the linear dispersion relation. Indeed, nonlinear dispersion relations require extremely accurate estimation of additional swell parameters, including wave height, which cannot be achieved by remote sensing or *in situ* data [47], [48]. Hence, the practical application of nonlinear theories involves such a high level of uncertainty that the overall uncertainty in water depth results to be higher than neglecting nonlinear processes [26]. For that reason and in agreement with recent literature results [24], [37], [38], the linear dispersion relation is selected as the most suitable one for SAR-based bathymetry in this work.

III. SAR Imaging of Swell Waves

The application of the linear dispersion relation for depth determination requires the knowledge of swell wavelength and period over the area of interest. In the present case, both the parameters have to be estimated using SAR data.

In general, wave patterns detected in SAR images are not the true waves, i.e., SAR image is not a picture of sea surface [42]. This is because the imaging mechanism of sea surface by SAR is not linear. Hence, contributions from different portions of sea wave spectrum combine in a nonlinear way to generate the final image. The main scatters are the shorter wavelengths matching Bragg's resonant condition [50]. As noted in the previous section, Bragg's waves are dominated by wind in terms of both speed and directionality. When swell waves propagate over sea surface, they modulate sea surface roughness, i.e., the distribution of Bragg's waves. Specifically, SAR imaging of swell waves is related to the mechanisms of hydrodynamic modulation, tilt modulation, and velocity bunching modulation [43]. For the present problem, the effect is important of velocity bunching for azimuth travelling swell waves. As azimuth waves grow steeper, the radial velocity increases, resulting in azimuth displacements due to Doppler effects. Depending on swell wavelength and SAR sensor parameters, specific conditions exist in which the azimuth displacement cannot be tracked by SAR, so image smearing is introduced. Smearing reduces the azimuth resolution and therefore limits the detectable sea surface wavelength. Empirical equations are available to estimate the so-called cutoff length, i.e., the minimum detectable wavelength of swell traveling along the azimuth direction [51].

Based on the above discussion, it is clear that complex models are necessary to retrieve sea spectrum information [28], [42], [52], [53]. Traditional solutions are based on a two-step model in which the behavior of shorter wavelengths is modeled in a forward approach based on a priori knowledge of wind field. The residual spectrum, i.e., the spectrum of longer wavelengths, is computed as the difference between the observed SAR spectrum and the estimated contribution from shorter wavelengths. Specific conditions exist in which this approach can be simplified notably [52], [53]. This is the case of nonextreme wind speed and sea state, the absence of surface currents and wind sea contributions, and swell patterns characterized by wavelengths that are sufficiently far from cutoff conditions, i.e., including 1) swell propagating along the range direction or 2) azimuth propagating swell significantly longer than the azimuth cutoff length due to velocity bunching. Under these conditions, experimental results [24], [54] indicate that there is a linear relation between the wavelengths derived by SAR and those measured by buoy. The results of the present paper concern this particular case. Nonetheless, the required conditions are not rare, so they can be successfully exploited to perform bathymetry.

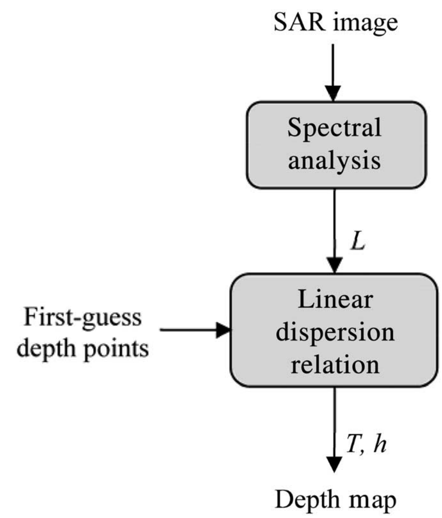

Fig. 1. Theory-driven algorithm for swell-based bathymetry [26], [37].

A. Image Analysis for Swell-Based Bathymetry

Based on the selected linear model, swell shoaling and refraction can be investigated and swell waves can be tracked from offshore up to the shoreline.

Fig. 1 depicts the main steps to be performed for L and T retrieval and for sea water depth estimation. This oversimplified algorithm assumes that swell waves are perfectly imaged by SAR without any source of perturbation. It is therefore called theory-driven algorithm in what follows. Sea surface spectrum is estimated by fast Fourier transform (FFT) of image intensity. The resulting peak in the 2-D spectrum reveals the dominant swell wavelength and the dominant swell direction of propagation in the considered portion of the SAR image. Hence, investigation of swell shoaling and refraction can be performed by scanning the region of interest with a small window and by executing the spectral analysis at each location within this small window. Fig. 2 shows a sketch of the raster scanning approach adopted in the present work. A scanning window is moved by a predetermined distance, or sampling step, along the range and azimuth directions, starting from offshore and until the shoreline. The FFT is applied on each subimage covered by the scanning window and the directional wave spectrum of the local swell field is retrieved. In this way, values of swell wavelength and direction of propagation are calculated over a regular grid throughout the area of interest. The retrieved swell direction of propagation has an ambiguity of 180°. However, in coastal area, this ambiguity problem can be solved by observing the SAR image and considering that swell waves propagate toward the coast [24].

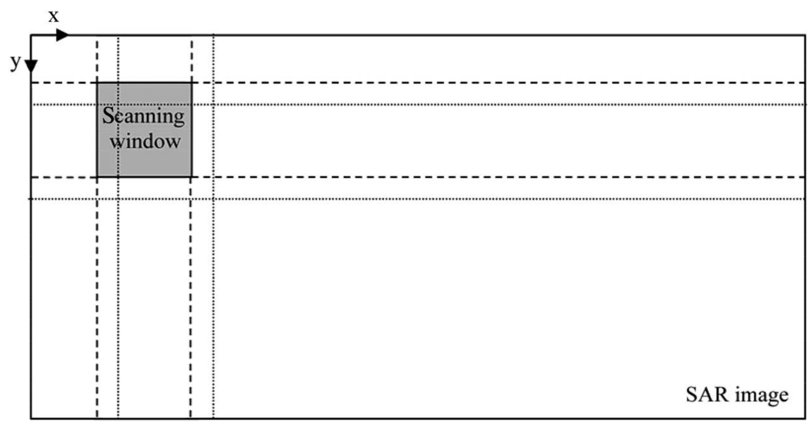

Fig. 2. Illustration of the raster scanning approach.

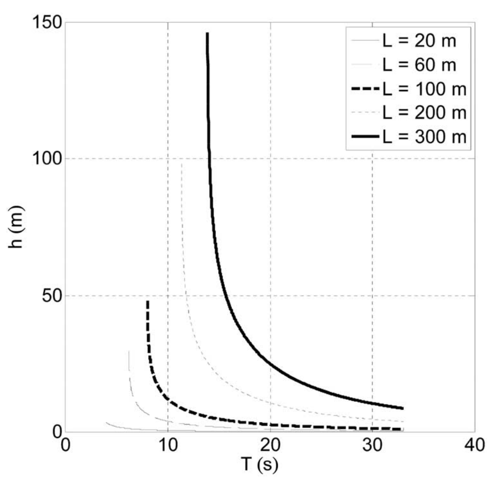

Fig. 3. Sea water depth as function of swell period for different values of swell wavelength as modeled by the linear dispersion relation theory-driven algorithm for swell-based bathymetry [26], [37].

Concerning swell period, it is well known that the period cannot be directly retrieved from a single SAR image [24], [37], [38]. The wave period could be measured from a temporal sequence of radar images [36], but this sequence is not typically delivered in satellite remote sensing application. If external sources, such as buoys or weather services are not available, the wave period can be measured by the dispersion relation starting from the knowledge of local depth in one or a few locations within the area of interest [37]. In detail, swell period is evaluated offshore by (1) using trial values of T and by comparing the obtained value with the actual water depth reported on available low-resolution topographic datasets, e.g., nautical maps. In general, such a kind of first-guess approach is of limited accuracy. However, an important property of the dispersion relation can be exploited. As shown in Fig. 3, when the wave period is sufficiently long and local depth quite small, the sensitivity of the depth to the wave period is very low and therefore high uncertainties on the wave period and wave period variations can be tolerated. The first-guess approach is typically applied as close as possible to the intermediate water depth area [24], [37], in order to further reduce potential water depth errors.

Finally, the theory-driven algorithm uses the values of L and T retrieved over the investigated area to estimate sea water depth according to (1). In this way, a dense and regular distribution of depth measurements is obtained and a bathymetric map can be generated.

IV. Bathymetric Algorithm

The validity of the linear imaging model does not guarantee the reliability of the theory-driven algorithm. Even if, from a global point of view, swell waves are correctly imaged and dominate SAR data, additional phenomena occur locally, including speckle, noise, and other sources of perturbation. Local estimation and tracking of swell by the theory-driven algorithm is thus extremely unstable and generally nonrobust. For this reason, the algorithm must be completed by further processing steps and procedures. Fig. 4 illustrates the proposed solution. It is based on the introduction of a preprocessing step before spectral analysis and a smoothing step after spectral estimation. Finally, the algorithm is completed by precise requirements and limitations posed to the outcomes of the frequency analysis.

Preprocessing is in charge of filtering out phenomena occurring at a smaller scale with respect to bathymetry. This is performed by resizing the original spatial resolution of SAR data, i.e., introducing a scaling factor. Standard bilinear interpolation is used to resize the image. The specific value of the scaling factor depends on the value of the original spatial resolution and should be set to reduce the noise without removing swell waves features on the SAR image. Thereafter, a 2-D median filter is applied on the resized image. The filter replaces the amplitude value of the resized SAR image pixels by the median value in the neighborhood around of any given pixel. Again, the kernel size of the median filter must be set to reduce the residual noise while preserving the image modulations generated by swell waves.

At this point, spectral analysis can be performed using the raster scanning approach (Fig. 3) and the FFT method to obtain the values of peak wavelength and peak wave direction along each track (see Section III). However, when the spectrum is computed in a relatively small box, at a given location over the image, not a single, dominant, peak is found, but several

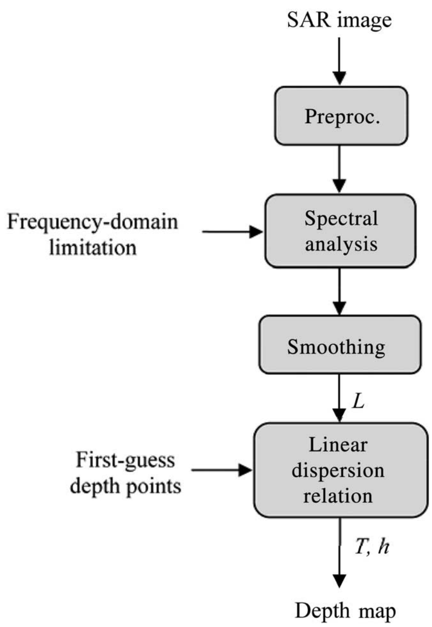

Fig. 4. Proposed algorithm for swell-based bathymetry.

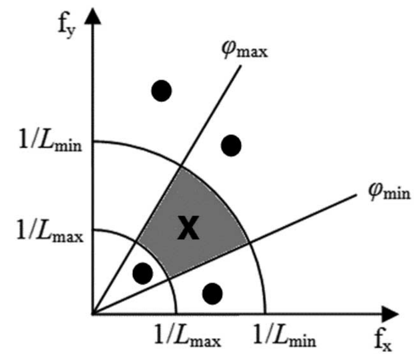

Fig. 5. As a result of the spectral analysis performed on a given small box, several peaks are obtained (marked with dots and cross on the image). Frequency-domain limitations on the (f_x, f_y) plane are set by the identified ranges of admissible swell wavelength ($[L_{min}; L_{max}]$) and angle of propagation ($[\phi_{\min}; \phi_{\max}]$). Only the peak included in the so-defined region of interest (i.e., gray area on the image) is considered (marked with a cross on the image) by the algorithm to perform wavelength and period estimation.

peaks appear (see Fig. 5). In order to select the right peak, i.e., the peak corresponding to swell waves to track, frequency-domain limitations are required. For this reason, the algorithm introduces a region of interest in the domain of the spectrum. The region of interest is a portion of a circular corona. Upper and lower boundaries of the corona guarantee that the retrieved peak wavelength is within the assigned range of typical swell wavelength, i.e.,

$$L_{\min} \leq \frac{1}{\sqrt{f_x^2 + f_y^2}} \leq L_{\max} \tag{2}$$

where $L_{\min}$ and $L_{\max}$ are the minimum and maximum expected wavelength and f_x, f_y are the spatial frequencies associated with the spectrum. The angular extent of the region can be instead defined introducing a range of admissible angles of propagation

$$\varphi_{\min} \leq \varphi \leq \varphi_{\max}, \quad \varphi = \tan^{-1}\frac{f_y}{f_x}. \tag{3}$$

The range of admissible angles, as well as the range of expected wavelengths, can be easily set looking at the SAR image (see Section V).

The last limitation to the spectrum analysis is the introduction of a maximum admissible deviation $\Delta\varphi$ of the propagation angle between two consecutive locations of the FFT box. This is useful to maintain the tracking of the main swell field and to avoid switching to wrong wave systems.

After completion of spectral analysis, a smoothing step is in charge of increasing the stability of the obtained results. This is achieved through a 2-D median filter processing the matrixes of wavelength and angle of propagation resulting from the spectral analysis. In addition, a moving average filter is applied along each row of the two obtained matrixes.

TABLE I
PARAMETERS OF THE PROCESSED ALOS PALSAR IMAGE

Parameter	Value
SAR signal band	L-band
SAR mode	Stripmap
Pixel spacing	6.25 m x 6.25 m
Range Looks	1
Azimuth Look 2	2
Acquisition epoch	Feb 13, 2007, 20:28 UTC
Incidence angle	~38.7°

At this point, the first-guess approach for wave period estimation can be applied and sea water depth can be derived by applying (1) for each location of the scanning window.

Overall, 11 parameters must be set to run the proposed algorithm: two parameters refer to the preprocessing steps (scaling factor and kernel size for median filter on the SAR image); two parameters define the raster scanning (i.e., FFT window size and sampling step); five parameters are required to introduce limitations to the output of the spectral analysis (i.e., maximum and minimum wavelengths and propagation angles, and maximum admissible deviation between consecutive boxes); and two parameters are used by the final smoothing step (kernel size of the median filter and span of the moving average filter). As shown in Section V-B, most of these tuning parameters can be set from visual image inspection.

V. Experimental Results

A. Study Area and Data

The described algorithm for swell-based bathymetry is applied to the ALOS PALSAR image covering the Gulf of Naples, Italy, whose parameters are listed in Table I. The processed image is a Level 1.5 product, i.e., a multilook image in ground range and azimuth coordinates [55]. Specifically, a subset of the original image is processed. The subset is shown in Fig. 6. It corresponds to the northern side of the Gulf of Naples, Italy, and covers an area of about $5\,\text{km} \times 4.8\,\text{km}$. The official

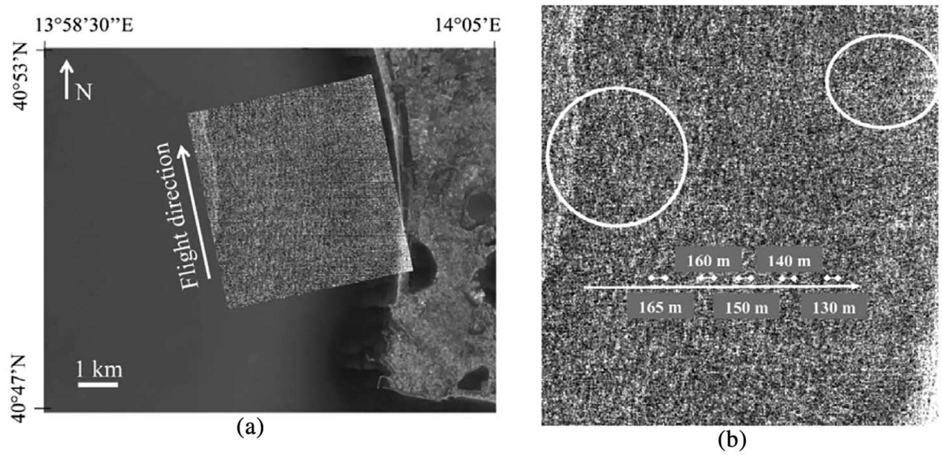

Fig. 6. (a) Subset of the ALOS stripmap image covering the northern side of the Gulf of Naples, Italy (background image Google Earth) whose parameters are listed in Table I. The subset covers an area of about 5 km × 4.8 km. (b) Values of swell wavelength retrieved from visual inspection at different locations along the ground range direction. Swell waves are propagating toward the coast (located on the right side). Two areas on the sea surface do not show prominent refraction and shoaling phenomena (marked by circles on the subset).

nautical chart of the Gulf of Naples delivered by the Italian Navy Hydrographic Institute [56] shows that seabed gradually varies in that region and water depth remains low even at a long distance from the shoreline. Nonsignificant weather phenomena were present at the time of image acquisition, and the wind speed was about 3 m/s [57]. Moreover, swell waves propagate close to the ground range direction and tend to become parallel to the shoreline. According to weather data and visual analysis, it can be concluded that the selected dataset is a good candidate to test both the linear imaging model and the proposed algorithm.

B. Results

As a result of the visual analysis [see Fig. 6(b)], the range of admissible wavelength and propagation angle are set to [50 m, 200 m] and [0°, 30°], respectively. Hence, the value of the scaling factor is set to lead to a degraded spatial resolution of about 15 m, which is still able to correctly sample the shortest admissible wavelength. As a consequence, the study area is covered by 40 tracks and a numeration is assigned so that the first track is the one laying alongside of the upper edge of the investigated area. Each track is set at a distance of five resized pixels from the upper edge of the previous one and the maximum deviation of the wave propagation direction between two consecutive FFT boxes is set to 15° [37], [38]. Further setting parameters are listed in Table II.

The application of the proposed algorithm results in values of swell wavelength and angle of propagation estimated throughout the subset. To highlight the achieved improvement in swell detection and investigation capabilities, Fig. 7(a) reports the retrieved L-peak values along a track of the study area, for both the case of application of the theory-driven and proposed algorithms. The estimated wavelength by the theory-driven algorithm is unstable, and extremely large, unrealistic, values (up to 2000-m long wavelength) are derived. This means that the spectral analysis is not tracking the desired wave field correctly. The application of preprocessing, smoothing, and limitations in the frequency domain keeps the wavelength more stable.

TABLE II
PARAMETERS OF THE PROCESSED ALOS IMAGE

Setting parameter	Value
Scaling factor	2.5
FFT window size	128 x 128 resized pixels
FFT window sampling step	5 resized pixels
$\Delta\varphi$	15°
Kernel size for median filter on the SAR image	5 x 5 resized pixels
Kernel size for median filter on the L and φ matrixes	5 x 5 elements
Moving average span	20 elements
$L_{\min}$	50 m
$L_{\max}$	200 m
$\varphi_{\min}$	0°
$\varphi_{\max}$	30°

Results show that the proposed algorithm provides L-peak values in the expected range for swell waves [24], [37], [38], and in agreement with the ones obtained from visual inspection of the processed image [see Fig. 6(b)]. Moreover, as expected, L-peak values decrease as approaching the coast. Hence, it is possible to state that swell waves are properly tracked. Similarly, Fig. 7(b) reports the trend for the swell angle of propagation related to the L-peak values reported in Fig. 7(a), for the case of application of both the theory-driven algorithm and the proposed algorithm. Again, implementation of the proposed algorithm provides values of swell angle of propagation consistent with the expected trend in the investigated area. Similar trends in swell wavelength and angle of propagation can be found for the other tracks covering the investigated subset.

Table III lists the values of swell period for each track calculated by the first-guess approach, using the obtained L-peak values and the reference water depth reported on the "Gulf of Naples" Nautical Chart [56].The closer the track is to the

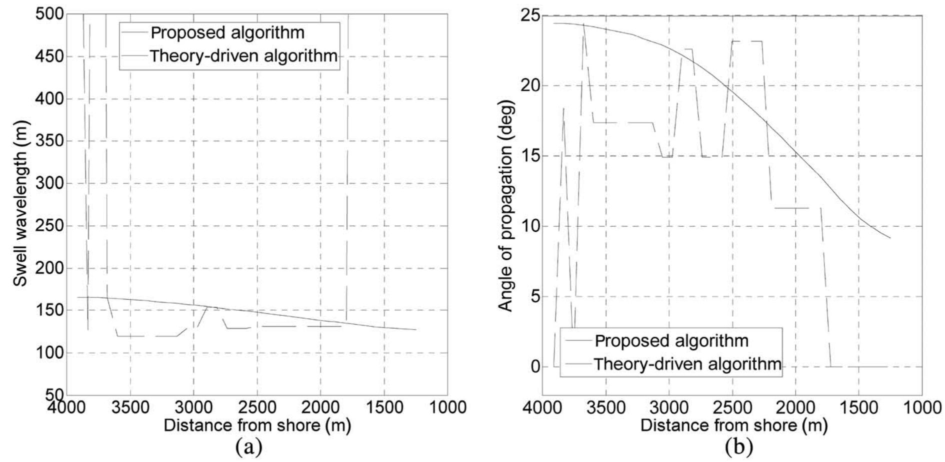

Fig. 7. (a) Retrieved L-peak and(b) angle of propagation along the 35th track of the investigated area.

TABLE III
VALUES OF SWELL PERIOD

Track number	T (s)
1–5	9.90
6–17	10.0
18–27	10.5
28–40	10.8

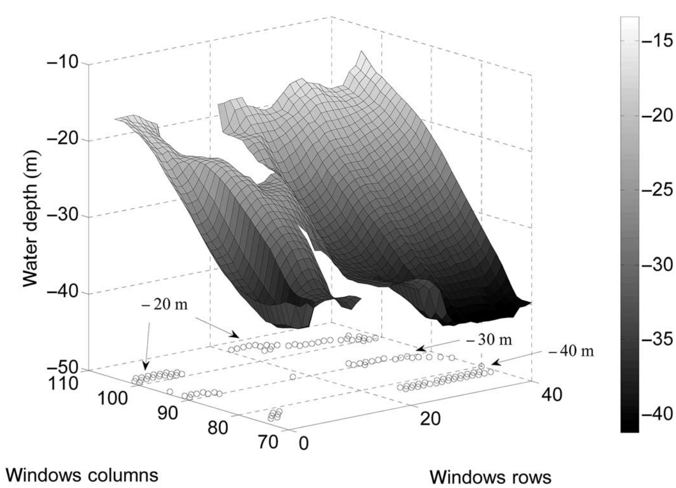

Fig. 8. Bathymetric map of the investigated area resulting from the application of the proposed algorithm for swell-based bathymetry by SAR imagery. Gray circle markers indicate the location of the control points extracted from the nautical chart and used to evaluate the accuracy of the generated map.

bottom edge of the investigated area, the larger the value of t is. This trend can be explained considering the presence of two channels, i.e., the Procida Channel and the Ischia Channel, beneath the investigated area. Channels generate significant hydrodynamic effects; hence, swell period may increase as approaching these areas.

Fig. 8 shows the resulting bathymetric map according to the estimated wavelengths and periods. Each track on the SAR image corresponds to a row in the retrieved sea water depth

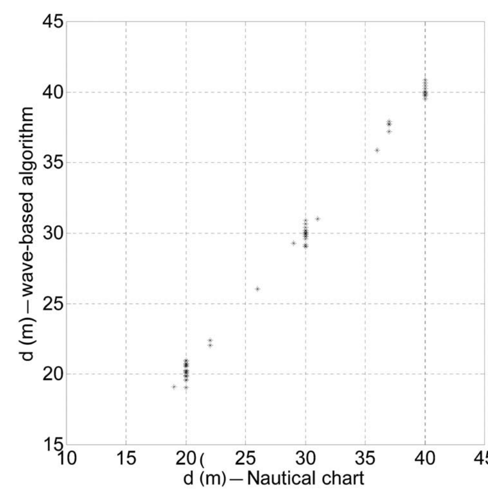

Fig. 9. Correlation analysis over the considered area of the ALOS image among the available control points of nautical chart and the corresponding values retrieved by the proposed algorithm.

matrix and each location of FFT box along the same track corresponds to a column along the same row. Two areas of the map are characterized by wrong values of sea water depth due to the presence of misleading features on the SAR image [see Fig. 6(b)]. Those areas in the original data set did not show prominent refraction and shoaling phenomena. Specifically, the offshore area was lacked of well-defined swell waves propagating on the sea surface, while the area closer to the coastline was affected by a wave-breaking process that destroyed the swell waves' propagation. Those areas are removed in Fig. 8.

The obtained results are in good agreement with the values of sea water depth reported in the official nautical chart. Fig. 9 shows a correlation analysis performed considering 108 control points available from the chart and the corresponding values estimated by the proposed algorithm. The correlation between the data is very high, the correlation coefficient being 0.99. The mean difference results to be about 0.2 m and the maximum difference is 0.9 m. Finally, the standard deviation of the difference is about 0.4 m.

VI. Conclusion

An algorithm has been proposed and tested for swell-based bathymetric data by SAR data. The algorithm relies on a linear imaging model and assumes that swell patterns imaged by SAR correspond to the true gravity wave patterns. However, it differs from the merely theory-driven approach because it includes additional steps to be performed to properly retrieve swell waves' characteristics and sea water depth. The proposed algorithm has been tested on ALOS data of the Gulf of Naples, Italy. The obtained results have been compared with the actual values of water depth reported in the official nautical chart. Comparison has shown that the method is able to successfully follow the behavior of bottom topography. Based on the indirect process through which bathymetry is sensed by SAR, only seabed features having scale length at least of the same order of magnitude as the peak wavelength of the local swell field can be identified. The presented bathymetric algorithm is thus suggested for gradually varying seabed without sharp depth variations. The adopted dispersion relation is valid in the range of intermediate waters. This range cannot be determined *a priori*, as it depends on the specific case, i.e., on the actual values of swell wavelength. Different swell fields can be thus sensitive to different bathymetric ranges and features. Planned future activities will deal with testing the proposed algorithm on different datasets, including COSMO-SkyMed X-band data.

Acknowledgment

ALOS data used in this work were made available by the Italian Space Agency under ASI Contract No. I/064/11/0.

References

[1] National Oceanic and Atmospheric Administration. (2015). *NOAA's Website* [Online]. Available: http://oceanservice.noaa.gov/facts/bathymetry.html

[2] Horizon 2020. (2014). *The EU Framework Programme for Research and Innovation* [Online]. Available: http://ec.europa.eu/research/horizon2020/

[3] S. Flampouris, "On the wave field propagating over an uneven sea bottom observed by ground based radar," Ph.D. dissertation, Dept. Earth Sci., Univ. Hamburg, Hamburg, Germany, Jul. 2010, 207pp.

[4] B. W. Eakins and L. A. Taylor, "Seamlessly integrating bathymetric and topographic data to support tsunami modeling and forecasting efforts," in *Ocean Globe*, J. Breman, Ed. Redlands, CA, USA: ESRI Press, 2010, pp. 37–56.

[5] International Hydrographic Bureau, "Depth determination," in *Manual on Hydrography*, 1st ed. Monaco, Monaco: International Hydrographic Bureau, May 2005.

[6] NOAA Ocean Exploration. (2013). *NOAA's Website* [Online]. Available: http://oceanexplorer.noaa.gov/history/timeline/timeline.html

[7] H. M. Dierssen and A. E. Theberge Jr., "Bathymetry: History of seafloor mapping," in *Encyclopedia of Natural Resources*. USA: Website of Coastal Ocean Lab for Optics and Remote Sensing, University of Connecticut, 2014 [Online]. Available: http://colors.uconn.edu/pubs/DIERSSEN-Bathymetry_history_LO.pdf

[8] H. K. Farr, "Multibeam bathymetric sonar: Sea beam and hydro chart," *Mar. Geod.*, vol. 2, no. 2, pp. 77–93, 1980.

[9] A. Guadagni, "Rilevamenti Marini e Batimetria," in *Prontuario dell'ingegnere*. Milano, Italy: Hoepli, 2010.

[10] J. Gao, "Bathymetric mapping by means of remote sensing: Methods, accuracy and limitations," *Prog. Phys. Geogr.*, vol. 33, no. 1, pp. 103–116, 2009.

[11] D. K. Burton, *Modern Radar System Analysis*. Norwood, MA, USA: Artech House, 1991.

[12] X. Lurton, *An Introduction to Underwater Acoustics—Principles and Applications*. Berlin, Germany: Springer-Verlag, 2002.

[13] J. C. Gibeaut, R. Gutierrez, and J. A. Kyser, "Increasing the accuracy and resolution of coastal bathymetric surveys," *J. Coastal Res.*, vol. 14, pp. 1082–1098, 1998.

[14] A. Renga *et al.*, "SAR bathymetry in the Tyrrhenian Sea by COSMO-SkyMed data: A novel approach," *IEEE J. Sel. Topics Appl. Earth Observ. Remote Sens.*, vol. 7, no. 7, pp. 2834–2847, Jul. 2014.

[15] H. M. Dierssen and A. E. Theberge Jr., "Bathymetry: Assessing methods," in *Encyclopedia of Natural Resources*. USA: Website of Coastal Ocean Lab for Optics and Remote Sensing, University of Connecticut, 2014 [Online]. Available: http://colors.uconn.edu/pubs/DIERSSEN-Bathymetry_Methods_LO.pdf

[16] S. Jay, M. Guillaume, and J. Blanc-Talon, "Underwater target detection with hyperspectral data: Solutions for both known and unknown water quality," *IEEE J. Sel. Topics Appl. Earth Observ. Remote Sens.*, vol. 5, no. 4, pp. 1213–1221, Aug. 2012.

[17] H. Abdallah, J.-S. Bailly, N. N. Baghdadi, N. Saint-Geours, and F. Fabre, "Potential of space-borne LiDAR sensors for global bathymetry in coastal and inland waters," *IEEE J. Sel. Topics Appl. Earth Observ. Remote Sens.*, vol. 6, no. 1, pp. 202–216, Feb. 2013.

[18] V. I. Feigels and Y. I. Kopilevich, "Lasers for lidar bathymetry and oceanographic research: Choice criteria," in *Proc. Int. Geosci. Remote Sens. Symp. (IGARSS'94)*, Aug. 1994, vol. 1, pp. 475–478.

[19] H. Parker and M. Sinclair, "The successful application of airborne LiDAR bathymetry surveys using latest technology," in *Proc. OCEANS*, May 21–24, 2012, pp. 1–4.

[20] J. M. Wozencraft, "Complete coastal mapping with airborne lidar," in *Proc. MTS/IEEE OCEANS*, Oct. 29–32, 2002, vol. 2, pp. 1194–1198.

[21] National Oceanic and Atmospheric Administration (NOAA) National Ocean Service. (2015). *What is LIDAR?* [Online]. Available: http://oceanservice.noaa.gov/facts/lidar.html

[22] National Oceanic and Atmospheric Administration (NOAA) Coastal Services Center, *Lidar 101: An Introduction to Lidar Technology, Data, and Applications*. Charleston, SC, USA: NOAA Coastal Services Center, 2012 (Revised) [Online]. Available: http://coast.noaa.gov/digitalcoast/_/pdf/lidar101.pdf

[23] National Oceanic and Atmospheric Administration (NOAA) Office of Coast Survey. (2015). *Lidar* [Online]. Available: http://www.nauticalcharts.noaa.gov/hsd/lidar.html

[24] A. Pleskachevsky, S. Lehner, T. Heege, and C. Mott, "Synergy and fusion of optical and synthetic aperture radar satellite data for underwater topography estimation in coastal areas," *Ocean Dyn.*, vol. 61, pp. 2099–2120, 2011.

[25] W. Alpers, G. Campbell, H. Wensik, and Q. Zhang, "Underwater topography," in *Synthetic Aperture Radar Marine User's Manual*, 1st ed. Washington, DC, USA: U.S. Department of Commerce, 2004, ch. 10, pp. 245–262.

[26] A. Renga *et al.*, "Analysis of SAR monitoring capabilities in coastal areas," in *Proc. IET Int. Conf. Radar Syst.*, Glasgow, Scotland, Oct. 2012, pp. 1–6.

[27] J. Vogelzang, G. J. Wensink, C. J. Calkoen, and M. W. A. van der Kooij, "Mapping submarine sand waves with multi-band imaging radar: 2. Experimental results and model comparison," *J. Geophys. Res.*, vol. 102, pp. 1183–1192, 1997.

[28] W. Alpers and I. Hennings, "A theory of the imaging mechanism of underwater bottom topography by real and synthetic aperture radar," *J. Geophys. Res.*, vol. 89, no. 10, pp. 529–546, 1984.

[29] J. Vogelzang, "Mapping submarine sand waves with multi-band imaging radar: 1. Model development and sensitivity analysis," *J. Geophys. Res.*, vol. 102, pp. 1163–1181, 1997.

[30] J. Inglada and R. Garello, "On rewriting the imaging mechanism of underwater bottom topography by synthetic aperture radar as Volterra series expansion," *IEEE J. Ocean. Eng.*, vol. 27, no. 3, pp. 665–670, Jul. 2002.

[31] J. Vogelzang, "The mapping of bottom topography with imaging radar. A comparison of the hydrodynamic modulation in some existing models," *Int. J. Remote Sens.*, vol. 10, no. 9, pp. 1503–1518, 1989.

[32] R. Romeiser, "Current measurements by airborne along-track InSAR: Measuring technique and experimental results," *IEEE J. Ocean. Eng.*, vol. 30, no. 3, pp. 552–569, Jul. 2005.

[33] C. J. Calkoen, G. H. F. Hesselmans, G. J. Wesink, and J. Vogelzang, "The bathymetry assessment system: Efficient depth mapping in shallow seas using radar images," *Int. J. Remote Sens.*, vol. 22, no. 15, pp. 2973–2998, 2001.

[34] H. Wensink and G. Campbell, "Bathymetric map production using the ERS SAR," *Backscatter*, vol. 8, pp. 17–22, 1997.

[35] A. Renga *et al.*, "Analysis of spaceborne SAR monitoring capabilities for coastal areas bathymetry with COSMO-SkyMed and ALOS data," in *Proc. SPIE 8888 Remote Sens. Ocean Sea Ice Coastal Waters Large Water Reg.*, 2013, vol. 888808, pp. 1–15.

[36] C. Wackerman, D. Lyzenga, E. Ericson, and D. Walker, "Estimating nearshore bathymetry using SAR," in *Proc. IEEE Int. Geosci. Remote Sens. Symp. (IGARSS'98)*, Seattle, WA, USA, 1998, vol. 3, pp. 1668–1670.
[37] S. Brusch, P. Held, S. Lehner, W. Rosenthal, and A. Pleskachevsky, "Underwater bottom-topography in coastal areas from TerraSAR-X data," *Int. J. Remote Sens.*, vol. 32, no. 16, pp. 4527–4543, 2011.
[38] M. K. Mishra, D. Ganguly, and P. Chauhan, and Ajai, "Estimation of coastal bathymetry using RISAT-1 C-band microwave SAR data," *IEEE Geosci. Remote Sens. Lett.*, vol. 11, no. 3, pp. 671–675, Mar. 2014.
[39] V. Boccia *et al.*, "Application of SAR data from Cosmo-SkyMed and ALOS for coastal area bathymetry in the Gulf of Naples," in *Proc. 22nd AIDAA Conf.*, Naples, Italy, Sep. 9–12, 2013, pp. 1–9.
[40] V. Boccia *et al.*, "L-band SAR image processing for the determination of coastal bathymetry based on swell analysis," in *Proc. IEEE Int. Geosci. Remote Sens. Symp.*, Québec City, Canada, Jul. 2014, pp. 5144–5147.
[41] V. Boccia *et al.*, "Seabed morphology retrieval in coastal areas from ALOS and COSMO-SkyMed SAR," in *Proc. Int. Astronaut. Conf.*, Toronto, Canada, Sep. 2014, pp. 1–8.
[42] K. Hasselman *et al.*, "Theory of synthetic aperture radar ocean imaging: A MARSEN view," *J. Geophys. Res.*, vol. 90, no. C3, pp. 4659–4686, May 1985.
[43] S. Robinson, *Measuring the Oceans from Space*. Chichester, U.K.: Springer/Praxis, 2004.
[44] *Coastal Engineering Manual*, 2nd ed. Vicksburg, MS, USA: U.S. Army Corps of Engineers, 2008, pp. II-1-1–II-1-106.
[45] G. J. Komen *et al.*, *Dynamics and Modelling of Ocean Waves*. Cambridge, U.K.: Cambridge Univ. Press, 1994, pp. 5–16, 343–349, 391–402.
[46] B. Kinsman, *Wind Waves, Their Generation and Propagation on the Ocean Surface*. New York, NY, USA: Dover, 1984.
[47] T. Kirby and R. A. Dalrymple, "An approximate model for nonlinear dispersion in monochromatic wave propagation models," *Coastal Eng.*, vol. 9, pp. 545–561, 1986.
[48] Y. K. Holland, "Application of the linear dispersion relation with respect to depth inversion and remotely sensed imagery," *IEEE Trans. Geosci. Remote Sens.*, vol. 39, no. 9, pp. 2060–2072, Sep. 2001.
[49] G. Main, *Vibrations and Waves in Physics*, 2nd ed. Cambridge, U.K.: Cambridge Univ. Press, 1988, pp. 210–253.
[50] F. T. Ulaby, R. K. Moore, and A. K. Fung, *Microwave Remote Sensing Active and Passive*. Reading, MA, USA: Addison-Wesley, 1982, vol. 2, pp. 841–842.
[51] B. Holt, "SAR imaging of the ocean surface," in *Synthetic Aperture Radar Marine User's Manual*, 1st ed. Washington, DC, USA: U.S. Department of Commerce, 2004, pp. 25–79.
[52] B. Chapron, H. Johnsen, and R. Garello, "Wave and wind retrieval from SAR images of the ocean," *Ann. Telecommun.*, vol. 56, pp. 682–699, 2001.
[53] F. Collard, F. Ardhuin, and B. Chapron, "Monitoring and analysis of ocean swell fields from space: New methods for routine observations," *J. Geophys. Res.*, vol. 114, no. C7, pp. 1–15, 2009, doi: 10.1029/2008jc005215.
[54] M. Buck and S. Lehner, "Sea state measurements using TerraSAR-X data," in *Proc. IEEE Int. Geosci. Remote Sens. Symp.*, Munich, Germany, Jul. 2012, pp. 7609–7612.
[55] *PALSAR's USER Guide*, 2nd ed. Tokyo, Japan: Japan Space Syst., Nov. 2012.
[56] *Gulf of Naples*, Nautical Chart, Italian Navy Hydrographic Inst., Genova, Italy, Ed., 1997, no. 127.
[57] Istituto Superiore per la Protezione e la Ricerca Ambientale (ISPRA). (2007). *Weather Data and Wind Speed Measurements at the Napoli Station of the National Tidegauge Network* [Online]. Available: mareografico.it

Valentina Boccia received the B.S. degree in aerospace engineering and the M.S. degree in aerospace engineering and astronautics from the University of Naples Federico II, Naples, Italy, in 2008 and 2011, respectively. She performed a 1-year internship in Thales Alenia Space, Rome, Italy, and she is currently pursuing the Ph.D. degree at the University of Naples Federico II.

Her research interests include the study and develop new technologies and solutions for remote sensing applications, with special emphasis on oceanography and bathymetry.

Alfredo Renga received the M.S. degree (*cum laude*) in aerospace engineering and the Ph.D. degree in industrial engineering from the University of Naples "Federico II," Naples, Italy, in 2006 and 2010, respectively.

He is currently an Assistant Professor with Aerospace System, School of Engineering, Naples, Italy. He held contracts and carried out research activities also with the Second University of Naples, the University of Naples "Parthenope," and with CO.RI.S.T.A., a private research consortium on advanced remote sensing systems led by Thales Alenia Space. He has authored more than 50 scientific papers (since 2007) published in distinguished international journals, conference proceedings, and book chapters, frequently referenced in international scientific and technical literature. His research interests include three-dimensional mapping by synthetic aperture radar (interferometry, radargrammetry, and bathymetry), maritime surveillance, and sea traffic monitoring by monostatic and bistatic SAR data, differential global positioning system (GPS) techniques for accurate relative navigation of aerospace platforms, design of hybrid bistatic and multistatic SAR systems for remote sensing and surveillance.

Dr. Renga was the recipient of the Second Prize in the Pegasus AIAA Conference in 2007.

Antonio Moccia (SM'09) received the M.S. degree in aerospace engineering from the University of Naples Federico II, Naples, Italy, in 1977.

He has been a Staff Scientist since 1983, and a Professor with Aerospace Systems, School of Engineering, Naples, Italy, since 1990. Since 1975, he has been holding grants and contracts from Italian State Agencies and Private and Public Industries in these fields. He has authored or coauthored more than 100 scientific papers and has been invited speaker and lecturer in international conferences and courses. He has been a Member of national and international committees and working groups and Principal or Co-Investigator of several national and international research programs. He is a Reviewer of international journals and of research proposals issued by national and international authorities. His research interests include aerospace high-resolution remote-sensing systems mission analysis, design, and data processing, as well as aerospace systems dynamics, guidance navigation and control.

Prof. Moccia has been a Member of the ORFEO Committee for Italian–French cooperation on space remote sensing as representative of the Italian Ministry for Research from 2002 to 2012, the scientific responsible of the Italian Space Agency for the Italian Bistatic and Interferometric Space Mission from 2005 to 2010, a Member of the Scientific Consulting Committee of the Italian Aerospace Research Center from 2010 to 2012, Co-Chair of the IAF (International Astronautical Federation) International Program Committee from 2010 to 2012. Considering his recent academic appointments, in 2001–2012, he has been a Chairman of the Ph.D. course in Aerospace, Naval and Total Quality Management Engineering, in 2006–2012, he has been a Chairman of study courses in Aerospace Engineering, and in 2007–2012, Chairman of the Ph.D. School in Industrial Engineering, University of Naples, Italy. Since 2013, he has been the Director of the Department of Industrial Engineering.

Simona Zoffoli received the M.S. degree in physics from the University of Rome "La Sapienza," Rome, Italy, in 1997, and the Ph.D. degree in geodesy and geomatics from Politecnico di Milano, Milan, Italy, in 2009.

As Program Manager, she has managed independently several programs aimed to develop applications based on Earth Observation space data to support activities of Italian Civil Protection related to volcanic and seismic risks. During her career, she has also been involved in many phase A studies for small scientific mission dedicate to study the Earth system.

Prof. Zoffoli is currently an ASI delegate to the ESA DOSTAG and to the CEOS WG Disasters.